J Mater Sci: Mater Electron (2016) 27:4913–4922
DOI 10.1007/s10854-016-4375-y

CrossMark

Sol–gel versus sputtering indium tin oxide films as transparent conducting oxide materials

M. Duta[1] · M. Anastasescu[1] · J. M. Calderon-Moreno[1] · L. Predoana[1] · S. Preda[1] · M. Nicolescu[1] · H. Stroescu[1] · V. Bratan[1] · I. Dascalu[1] · E. Aperathitis[2] · M. Modreanu[3] · M. Zaharescu[1] · M. Gartner[1]

Received: 30 October 2015 / Accepted: 18 January 2016 / Published online: 27 January 2016
© Springer Science+Business Media New York 2016

Abstract The aim of this paper is the replacing of the expensive sputtering method with the low cost sol–gel one in TCO applications. To this end two sets of indium tin oxide (ITO) thin films are compared and discussed in this paper: one obtained by r.f. sputtering and one by the sol–gel technique and dip-coating. For each of these sets of samples, a series of deposition parameters have been varied in an effort to obtain the most promising optical and electrical properties. Comparative structural, morphological and opto-electrical characterization of sol–gel and sputtered ITO-based films was performed by X-ray diffraction, Scanning electron microscopy, Atomic force microscopy, Spectroellipsometry, UV–VIS Spectroscopy and Hall Effect measurements in order to establish whether the chemical deposition method could lead to thin films with competitive properties as those obtained through the physical method. Comparable, high transmittance (85–90 %) in the VIS–NIR range (250–1050 nm) and carrier concentration values (10^{20}–10^{21} cm^{-3}) were obtained between sputtered and sol–gel ITO films. The sputtered ITO film in 75 % N_2, annealed at 500 °C and the sol–gel 0.1 M ITO film with 10 layers deposited on SiO_2/glass exhibit degenerate semiconductor behavior.

✉ M. Anastasescu
manastasescu@icf.ro

✉ H. Stroescu
hstroescu@icf.ro

[1] Institute of Physical Chemistry "Ilie Murgulescu", Romanian Academy, 202 Splaiul Independentei, 060021 Bucharest, Romania

[2] FORTH-IESL, Crete, Greece

[3] Tyndall National Institute, University College, Cork, Ireland

1 Introduction

Indium tin oxide (ITO) is the most well-known and utilized transparent conductive oxide (TCO), but also, the most expensive. Its special properties (high transmission above 90 %, low resistivity, n-type degenerate semiconductor behavior and wide direct band gap of ~3.6 eV) [1] make it suitable for a number of applications, such as electrochromic devices, liquid crystal displays, plasma displays and solar cells [2–6].

Multiple techniques have been used to fabricate ITO films, such as electron beam evaporation [7], chemical vapor deposition [8], pulsed laser deposition [9, 10], etc. Among all, r.f. sputtering [11–13] is employed, despite its high cost because of the quality of the resulting samples. Therefore it is challenging to develop low-cost TCO-based films, prepared by wet chemical methods (sol–gel [14], spray pyrolysis deposition [15, 16]) for photovoltaic devices on glass substrate, as well as to improve the energy conversion efficiency of these cells by post-crystallization treatments. The sol–gel method [17] is a versatile alternative to the sputtering technique, with an easier setup and a lower temperature budget. The great advantage of the sol–gel method is the possibility to cover large surfaces (such as windows) with uniform, nanosized films.

The aim of this work was to establish whether a chemical deposition method (sol–gel) could lead to thin films with competitive opto-electrical properties as those obtained through a physical method (r.f. sputtering).

2 Experimental

2.1 Film preparation

In this paper two types of ITO films deposited by a physical (r.f. sputtering) method in comparison with a chemical one (sol–gel) were studied.

The sputtered ITO thin films were deposited from an indium-tin-oxide (In_2O_3:SnO_2 = 8:2) target in 100 % N_2 or alternatively in a mixture of Ar and N_2 plasma (75 % N_2–25 % Ar) on fused silica. After deposition, the films were thermally treated by RTA for 1 min at 400, 500 and 600 °C. By studying the influence of the *deposition atmosphere* and *annealing temperature* on the structural, morphological and opto-electrical properties of the sputtered ITO films, the most promising sample in the series was identified [11].

The sol–gel ITO films were prepared on glass, and SiO_2 covered glass (further noted as SiO_2/glass), based on previous published results [18]. Solutions with 0.1 and 0.25 M concentrations were investigated (denoted from here on as 0.1 and 0.25 M ITO). At a withdrawal rate of 5 cm/min, films with 1–10 layers could be obtained from the 0.1 M solution, while only 1–5 layers were deposited from the 0.25 M solution due to its higher viscosity that leads to faster gelation. The viscosity of the 0.1 and 0.25 M solution was 1.37 and 1.47 respectively, as determined by a Brookfield Viscosimeter DV-II+Pro at room temperature in 8 mL solution.

Consolidation treatment (260 °C–10 min) was applied to the films after each deposited layer while a final annealing (400 °C–2 h) was applied after the last deposition. By studying the influence of the *solution concentration*, *number of layers* and *substrate type* on the structural, morphological and opto-electrical properties of the sol–gel ITO films, the most promising sample in the series was identified and compared to its sputtered counterpart [18].

2.2 Film characterization

The structure of the thin films was determined by X-ray diffraction, thin film method. The asymmetrical reflection measurements were performed with an Ultima IV diffractometer (Rigaku Corp., Japan), equipped with parallel beam optics and a thin film attachment, using Cu Kα radiation ($\lambda = 1.5405$ Å), operated at 30 mA and 40 kV, over the range $15 < 2\theta < 85°$, at a scanning rate of 1°/min and at a glancing angle ($\omega = 0.5°$) to determine both surface and near-surface structures. The crystallite size was estimated by the Scherrer equation from the broadening of the (222) diffraction line of the ITO phase, using the formula, [19]:

$$D = \frac{K\lambda}{\beta \cos\theta} \quad (1)$$

where D is the mean size of the ordered crystalline domains, which may be smaller or equal to the grain size; $K = 0.94$ is a dimensionless shape factor or Scherrer constant; λ is the X-ray wavelength; β is the line broadening at half the maximum intensity (FWHM), in radians and θ is the Bragg angle. The lattice parameters, $a = b = c$, of the ITO cubic structure were calculated from the X-ray diffraction lines position of lattice plane reflections (*hkl*). In the cubic crystal structure, for (222), (440) and (622) lattice plane distances, the lattice parameter value was calculated from the formula [19]:

$$\frac{1}{d^2} = \frac{h^2 + k^2 + l^2}{a^2} \quad (2)$$

Morphology and thickness of ITO films was obtained in top view and tilted view scanning electron microscopy (SEM) images, obtained using a FEI Quanta 3D microscope operating at 5 kV.

Atomic force microscopy (AFM) measurements were carried in the non-contact mode, with an XE-100 apparatus from Park Systems, using sharp tips. The topographical 3D AFM images were taken over the area of 2 × 2 μm^2. The images were processed with XEI (v.1.8.0) Image Processing Program developed by Park Systems regarding the tilt correction and the evaluation of the root mean square roughness and particle mean diameter.

Thickness (d) and the optical constants used to calculate the porosity (P) of the films were obtained by ellipsometric measurements with a J.A. Woollam Co. Inc. for UV–VIS–NIR range. Measurements were performed at room temperature, using 70° as incidence angle with 10 nm wavelength step.

The transmission (T) of the films was obtained by UV–VIS spectroscopy, with a Perkin Elmer—Lambda 35 apparatus in the 250–1050 nm spectral range. The optical band gap (E_g) was obtained from the transmission spectra, by first calculating the absorption coefficient, α, according to the formula [20]:

$$\alpha = \frac{1}{d}\ln\left(\frac{1}{T}\right) \quad (3)$$

where d is the film thickness as determined by spectroellipsometry and T is the transmittance of the film. Next, the plot of $(\alpha h\nu)^2$ versus the photon energy $h\nu$ was obtained, using [20]:

$$(\alpha h\nu)^2 = A(h\nu - E_g) \quad (4)$$

The E_g value was determined by the extrapolation method: the photon energy at the point where $(\alpha h\nu)^2 = 0$ represents E_g.

Electrical measurements based on the Hall effect, were performed on an HMS-5000 equipment from Ecopia using the van der Pauw method.

3 Results and discussion

3.1 Correlation between sample crystallinity and electrical properties

Indium oxide exists in two different crystallographic structures (rhombohedral and cubic), but high electrical conduction is normally achieved by the stabilization of the cubic phase [21, 22]. This is due to the distribution of Sn ions in the In_2O_3 lattice which lead to the formation of complexes involving interstitial oxygen ($2Sn^{\cdot}_{In}O''_i$) which, when reduced, give 2 free electrons [23].

It was observed that the ITO sputtering films are amorphous even after RTA as high as 500 °C, while the sol–gel ITO films are crystalline (Fig. 1b, c). However, annealing the sputtered thin films at 600 °C leads to crystalline, cubic structure (Fig. 1a).

a) The crystallinity of ITO films prepared by sputtering, starting from oxide targets is influenced by the oxygen partial pressure (pO_2) which in turn affects the oxygen content [24]. Crystallinity increases at higher pO_2, reaches a maximum value and then decreases with excess oxygen in the discharge gas (>25 %) [25, 26]. The deposition parameters, particularly the oxygen-free chamber atmosphere, consisting of reactive gas (N_2) mixed with inert gas (Ar), as described in the experimental section, lead to the obtaining of ITO films in amorphous state.

The crystallinity of ITO films deposited at low substrate temperatures is correlated with the total pressure, P_{tot} in the sputtering chamber. As the total pressure increases, the kinetic energy of sputtered atoms decreases as a result of the collision scattering. When the sputtered particles are not energetic enough for the enhancement of the surface migration, an amorphous structure of ITO films is obtained [27]. A degradation in crystallinity of the films caused by bombardment of high-energy particles will take place at very low P_{tot} (8.9×10^{-3} Pa) [28].

The degree of crystallinity of the films and the deposition rate decreased as the target-substrate distance decreased. The substrate temperature influences the grain size of ITO film sample, as the substrate temperature increases, the grain size along the substrate surface increases [29].

According to ICDD file no. 01-089-4596, the sputtering films annealed at 600 °C exhibit the reflections of the polycrystalline tin doped indium oxide, with no preferred orientation. No secondary phase of tin-based compounds was detected, which indicates that the tin atoms are doped substitutionally into the indium oxide lattice. The similar diffractograms of the films obtained in 75 and 100 % N_2 suggest that the influence of the *RTA temperature* on sputtered films structure is stronger than that of the deposition atmosphere.

b) The ITO thin films deposited by dip coating starting from the sol–gel solution are polycrystalline. The crystallite size and the crystallinity of the samples are influenced by the *precursor solution concentration,* the *substrate nature* and the *number of deposited layers*. The films deposited from the 0.25 M solution present a low crystallinity degree and small crystallite size. The films deposited from 0.1 M solution concentration exhibit a higher level of crystallinity, which increases with the number of layers and the afferent intermediate consolidating thermal treatment.

The different substrates (glass and SiO_2/glass) lead to different crystal lattice mismatch between substrates and ITO films which cause stress. In both cases, this is evidenced by the reduction in lattice plane spacing. Increasing the *number of layers*, the lattice constants approach the standard value (10.1234 Å—ICDD file no. 01-089-4596) and a lattice relaxation takes place due to consolidation thermal treatment after depositions. The influence of the

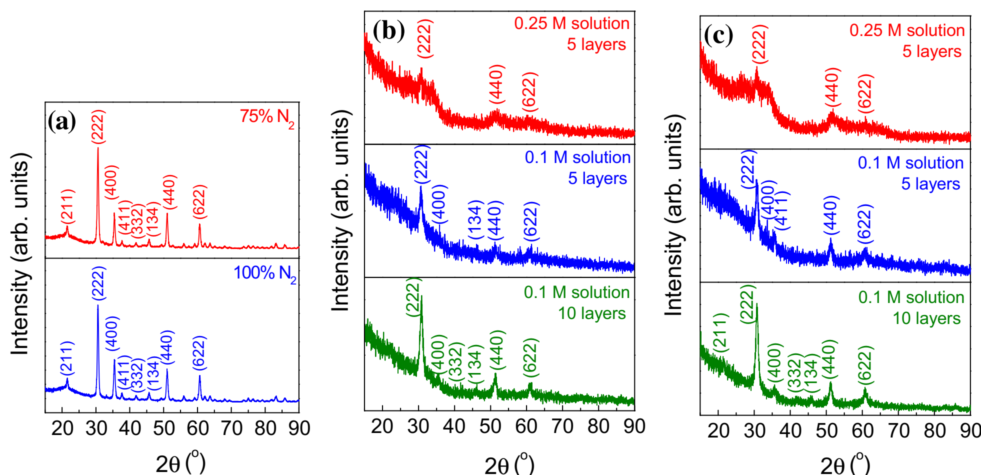

Fig. 1 XRD diffractograms of ITO sputtering films deposited on fused silica and RTA at 600 °C in 75 % N_2 and in 100 % N_2 (**a**) in comparison with the ITO sol–gel films TT at 400 °C and deposited on glass (**b**) and SiO_2/glass (**c**)

Table 1 Lattice constants and crystallite size of ITO sol–gel films

Substrate	No. of layers	Molar concentration (M)	2θ (°)	Lattice constants a = b = c (Å) α = β = γ = 90°	Crystallite size (nm)
SiO_2/glass	5	0.25	30.61 (12)	–	6.3 (12)
SiO_2/glass	5	0.1	30.69 (5)	10.0816 (2)	9.9 (13)
SiO_2/glass	10	0.1	30.75 (2)	10.10672 (17)	10.6 (3)
Glass	5	0.25	30.65 (11)	–	7.6 (26)
Glass	5	0.1	30.72 (7)	9.9483 (18)	9.1 (9)
Glass	10	0.1	30.86 (3)	10.0715 (4)	9.7 (3)

substrate type on the crystallite size of the samples is pronounced. As calculated by the Debye–Scherrer equation for the (222) diffraction line (Table 1), the crystallite size of the samples deposited on glass substrate is slightly smaller (9.1 nm) than for SiO_2/glass substrate (9.9 nm), especially when starting from 0.1 M solution.

It is expected that the crystalline ordering should directly affect the electrical properties of the films due to the carrier mobility. Thus, a larger crystallite size implies a smaller number of crystallites and, through this, a smaller number of grain boundaries where potential scattering and recombination may occur. This was not the case for the investigated ITO samples, suggesting that grain boundary scattering does not significantly affect the carrier mechanism. In order to confirm this assumption, the mean free path of the electrons was calculated, using the following formula [30, 31]:

$$l = \mu\left(\frac{h}{2e}\right)\left(\frac{3N_D}{\pi}\right)^{1/3} \quad (3)$$

where l is the mean free electron path, h is Planck's constant (6.626×10^{-34} $m^2kg\ s^{-1}$), e is the elementary charge (1.6021×10^{-19} C), N_D and μ are the carrier concentration and mobility as obtained from the Hall measurement. The mean free path values obtained are one order of magnitude lower than the crystallite size, confirming that grain boundary scattering is not the primary cause of low carrier mobility, in agreement with Chen et al. [30]. The low mobility values combined with the high carrier concentration (obtained for samples with 0.1 M concentration and 10 depositions) suggest a high recombination rate.

3.2 Correlation between surface morphology and electrical properties

Sol concentration, *substrate type* and *number of layers* all have a direct influence on the morphology of the sol–gel ITO samples [18].The electrical conductivity could not be determined for the 1 and 2 layers ITO sol–gel films because they are not continuous and exhibit porous islands, as seen in Fig. 2a–c for different magnifications. Continuous films can be observed for the five layer samples (Fig. 2d), establishing a clear influence of the *number of layers* on sol–gel ITO morphology.

The thicknesses determined from SEM analysis are in good agreement with the thickness obtained by ellipsometric measurements as illustrated for selected samples in Table 2. The *sol concentration* has a direct influence on the thickness and porosity of the films. The sol–gel films obtained from 0.25 M initial solution (Fig. 3d) are generally thicker than those obtained from 0.1 M (Fig. 3c) by as much as one order magnitude and can even reach the thickness of the sputtered ITO films (Fig. 3a, b) after five depositions. The porosity of the films follows a different trend: films obtained from the 0.25 M solution exhibit consistently higher values than those obtained from 0.1 M solution or those obtained through sputtering (Fig. 3a–d). This is due to the different viscosities of the solutions. For the less concentrated sol, the lower viscosity leads to better wetting of the substrate (for the first deposition) and of previously deposited layers (for multilayers) which promotes flat, smooth films. The 0.25 M sol, being more viscous, promotes film growth perpendicular to the substrate and leads to high porosity and roughness.

The influence of the *substrate type* may be linked to reactivity. While the SiO_2 layer acts as a suitable buffer against impurity diffusion from glass to film, it also increases the reactivity of the substrate, potentially increasing the coarseness of the films [18]. In Fig. 3d the stratification of the SiO_2/glass substrate is very clear, showing the ITO films on SiO_2 layer ($\sim$50 nm thick) on glass—the darker phase.

Thickness and *porosity* both play an important role in the electrical properties of thin films. Thinner films can sometimes exhibit lower electrical performance due to the combined effects of: low degree of crystallization, surface scattering and charge carrier trapping [32]. Porosity and roughness also link to this effect as higher values usually lead to increased surface scattering and lower mobility.

The high porosity shown in SEM images for the films with 0.25 M—5 layers on SiO_2/glass is also found in the

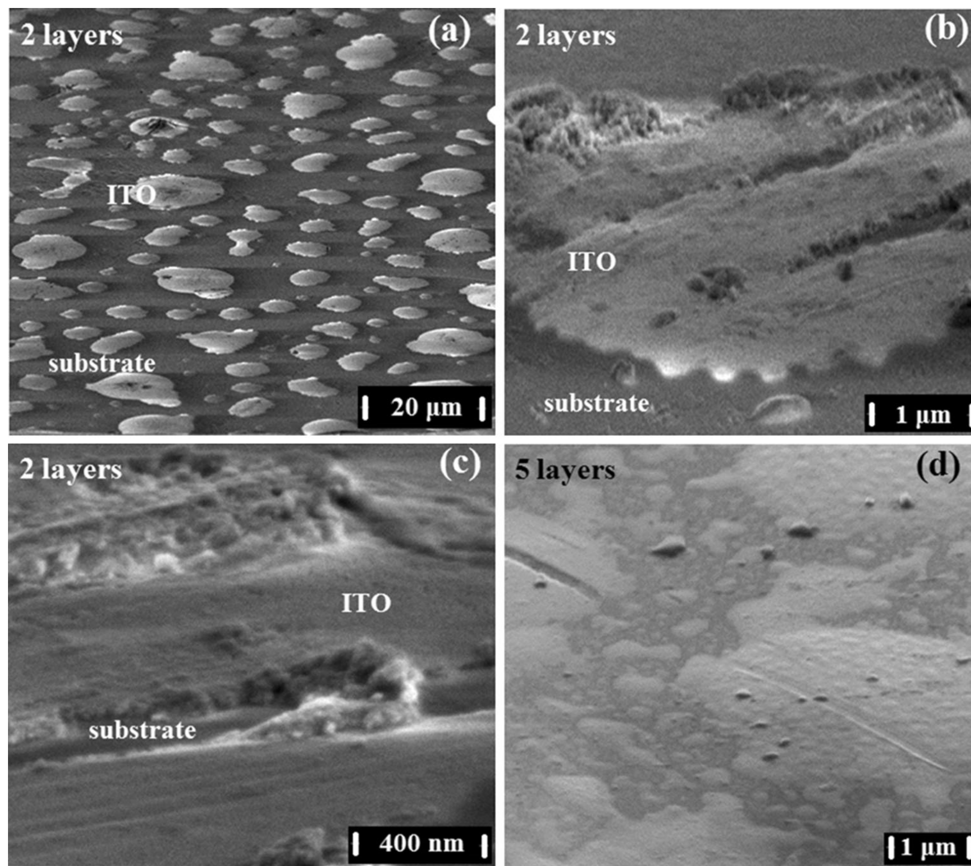

Fig. 2 Top view SEM images of 0.1 M film deposited on SiO_2/glass: *2 layers* with different magnifications (**a**–**c**); *5 layers* (**d**)

Table 2 Film thickness (d), optical band gap (E_g) and porosity (P)

Sample	d_{film} (SE) ± 2 nm	d_{film} (SEM) ± 20 nm	E_g (eV)	P (%)
75 %N_2- 500 °C/fused silica	254.0	250	3.68	10.00
100 %N_2- 500 °C/fused silica	381.0	390	3.80	2.84
0.1 M - 10 layers/SiO_2/glass	31.1	40	3.74	11.19
0.1 M - 15 layers/SiO_2/glass	59.0	–	3.87	9.28
0.25 M - 5 layers/SiO_2/glass	205.4	200	3.64	19.28

values calculated from refractive indices determined from ellipsometric measurements, using the relation:

$$P = \left(1 - \frac{n^2 - 1}{n_d - 1}\right) \times 100(\%) \quad (4)$$

where n is the refractive index of the film and n_d (=1.92 for $\lambda = 500$ nm) is pore-free ITO [33]. As can be seen from Table 2, more porous films are obtained by sol–gel deposition (11–19 %) in comparison with the films prepared by sputtering (2–10 %).

The 3D-topographic AFM images are shown in this paper at the scale of 2 × 2 μm^2 only for the ITO films prepared by sputtering and thermally treated at 600 °C (Fig. 4a, b). The r.f. sputtered ITO films are uniform and smooth up to 500 °C as we previously reported [11] exhibiting a continuous structure of small (10 nm) circular grains. After annealing at 600 °C, the surface of the sputtered ITO films is already defected, as can be seen from Fig. 4a, by the formation of pits (samples prepared in 75 % N_2) or even micro-cracks—Fig. 4b—(samples prepared in 100 % N_2). The roughness is also small and decreases with the temperature of RTA treatment up to 500 °C (Fig. 5a). At the RTA temperature of 600 °C, the roughness suddenly increases in both series of sputtered films (75 and 100 % N_2) because of some defects (10–15 nm deep) that accompany the crystallization process (as proved from XRD—Fig. 1a) which could induce mechanical stress in the films matrix.

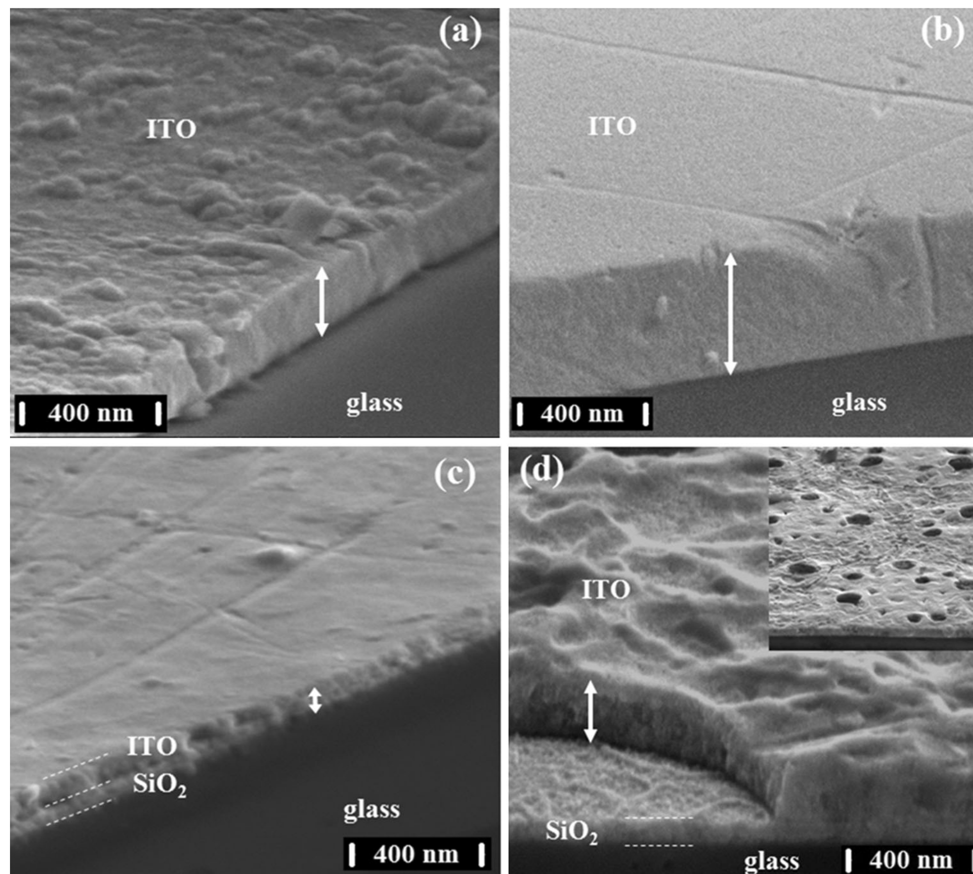

Fig. 3 Tilted view SEM images of ITO sputtering RTA at 500 °C obtained in 75 % N_2 (**a**) and 100 % N_2 (**b**) and sol–gel films with 0.1 M– 10 layers (**c**) and 0.25 M– 5 layers (**d**). *Insertion* in the Fig. 3d is a *top view* of the 0.25 M– 5 layers on SiO_2/glass

Along with the roughness variation with *RTA temperature*, the mean grain diameter of the sputtered films shows a similar trend (slightly larger for the films prepared in 100 % N_2), with a minimum at 500 °C followed by the formation of larger particles after crystallization at 600 °C. Only few particle aggregates are formed during RTA treatment (i.e. ITO—75 % N_2, 600 °C) which is due to the short annealing time. The *deposition atmosphere* plays a much smaller role than the *RTA temperature*, from a morphological point of view. The films deposited in 100 % N_2 are characterized by slightly smaller grain size and roughness values (Fig. 5a, b) which affect the electrical transport mechanism due to surface scattering and recombination processes. The samples prepared in 75 % N_2, which exhibited promising electrical properties, showed a decrease of the electrical resistivity from AP stage up to 500 °C accompanied by an increase in charge carrier density (Fig. 5d). Taking into account the roughness and mean diameter vs. RTA curves, this suggests a better intergranular transport. At 600 °C due to the crystallization process, some structural rearrangements take place and the appearance of surface defects (pits and micro-cracks) disturbed the grain boundaries contact which further affects the electrical properties (i.e. mobility and resistivity). The deterioration of the electrical behavior cannot be offset by the increased level of crystallinity, as previously stated in Sect. 3.1, which is an indicator of better structural ordering. This confirms that the morphology of the sputtered ITO films has a stronger effect on their electrical properties, compared to their structure. The increase in charge carrier density with the RTA temperature may have two sources of electron donors: the substitutional tin atoms and the oxygen vacancies. The carrier concentration (N_D) increasing with the oxygen vacancies is also supported by the Hall mobility (small) decrease from 400 to 500 °C for ITO films prepared in 75 % N_2 [11] as the mobility is very sensitive to defects density inside the films.

For the sol–gel films, the resistivity trend should follow the roughness and porosity trend and therefore be influenced by *solution concentration*, *substrate type* and *layer number*. The formation of large cavities for multilayered films prepared from 0.25 M ITO sol, as stated in a previous work [18] is accompanied by substantially higher resistivity values compared to those of the sol–gel 0.1 M films

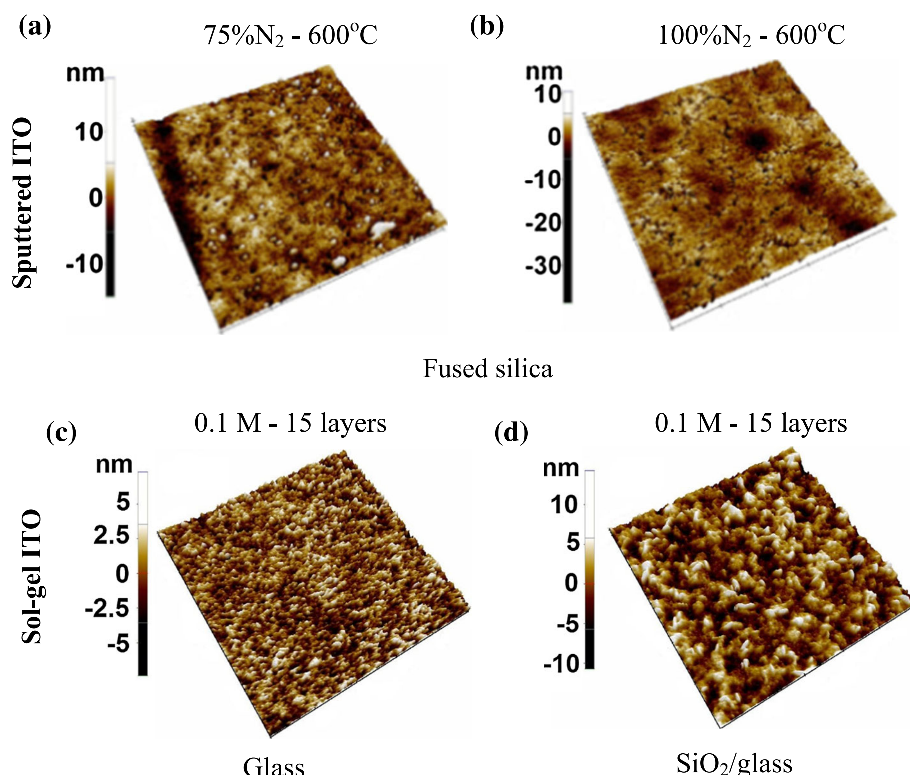

Fig. 4 Selective 3D-topographic AFM images comparatively presented at the scale of 2 × 2 μm^2 for ITO films prepared by sputtering (**a** and **b**) and sol–gel 0.1 M (**c** and **d**)

(Fig. 5g, h) which can be linked to the decreased charge carrier density. In this paper, the 3D AFM images of the 0.1 M sol–gel films with 15 layers (Fig. 4c, d) are presented, which show homogeneous surfaces but with larger superficial particles for the ITO films deposited on SiO_2/-glass as compared to those on glass substrate. The resistivity variation with the *number of layers* for the 0.25 M films follows the same trend as the roughness behavior (Fig. 5e, g). Instead, the films deposited from 0.1 M ITO sol show a trend of decreasing roughness and defects density by multiple depositions and thermal treatments (Fig. 5f) which favors the densification process and a decrease in resistivity or increase of the charge carrier density (Fig. 5h). The corresponding relatively low mobility suggests a high recombination rate. This could be attributed to impurity scattering while grain boundary scattering is less likely to significantly affect the carrier mechanism (as previously stated, the electron mean free path is much lower than the crystallite size).

The most promising electrical results were registered in Fig. 6 for both types of samples obtained by sputtering and sol–gel, which showed degenerate semiconductor behavior (carrier density is constant during temperature variation, $\Delta T = 110$–350 K) in Hall Effect measurements. In order to determine the optimal thickness for ITO thin films which exhibit the most promising electrical and optical properties, additional sol–gel films with 0.1 M—15 and 20 layers (approximately 60 and 70 nm thick, respectively) were deposited on SiO_2/glass substrate. Among the sol–gel samples (with 10, 15 and 20 depositions) shown in Fig. 6, the 0.1 M ITO—10 layers presents the highest carrier density and it is situated between the values obtained for 75 and 100 % N_2 sputtering films. The same behavior is also observed for the transmission spectra (Fig. 7).

It should be noted that the samples obtained through sol–gel from 0.1 M sol were generally much thinner than those deposited through r.f. sputtering. This could explain the slightly lower electrical performance of the former by as the combined effect of surface scattering and electron trapping. Even so, the deposition of more than 10 layers does not significantly improve the opto-electrical properties (carrier density and transmission) as seen from Figs. 6 and 7.

3.3 Transmission

Transmission is one of the clue points in obtaining of a good TCO material. The spectra of the UV–VIS optical transmission for all studied samples are presented in Fig. 7. A comparable transmittance (85–90 %) from 450 to 1050 nm spectral range was observed from both types of ITO films. Due to the fact that one layered ITO sol–gel films are very thin (∼20 nm) they are transparent regardless of their structural and morphological properties (see Fig. 7), but the

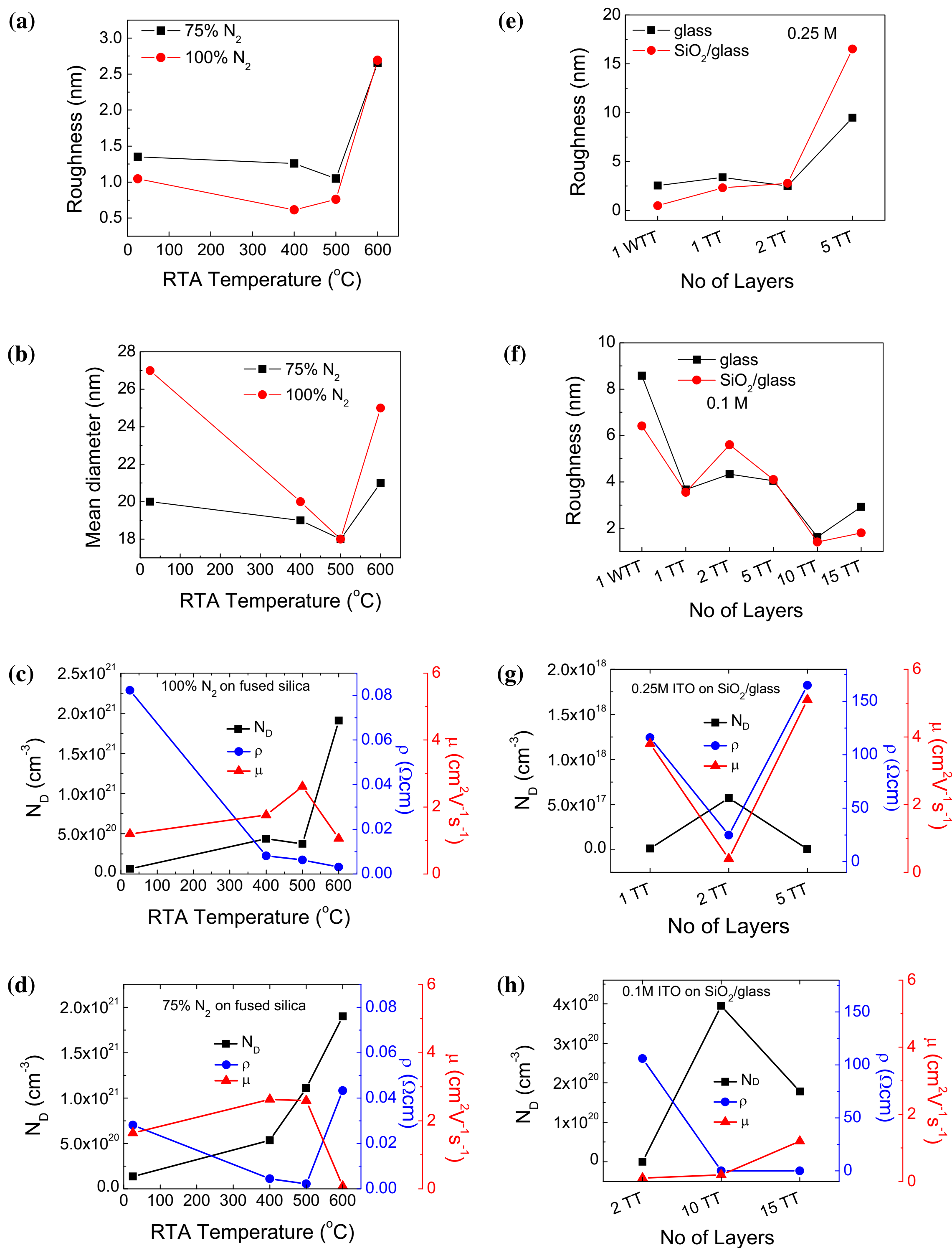

Fig. 5 Roughness (**a**, **e**, **f**), mean diameter (**b**), carrier concentration—N_D, resistivity—ρ and mobility—μ (**c**, **d**, **g**, **h**) of sputtered (*the first column*) and sol–gel films (*the second column*)

carrier number is too low (the transmission does not decrease in near infrared spectral range) to exhibit good electrical properties. Only after 10, 15 or 20 depositions can they be considered competitive with sputtering films.

Optical band gap (E_g), one of the three important parameters of a good TCO material (along with transmittance and carrier concentration) must be higher than 3.3 eV (lower than 380 nm). The values obtained in the frame of this work,

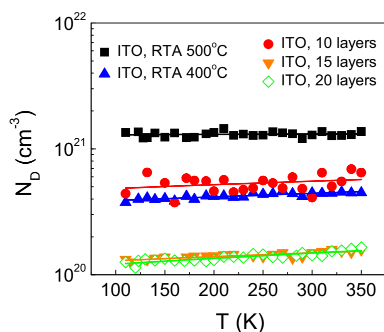

Fig. 6 The carrier concentration variation with temperature ($\Delta T = 110$–350 K) for sputtered (75 % N_2, RTA 500 °C and 100 % N_2, RTA 400 °C) in comparison with sol–gel (0.1 M– 10, 15 and 20 layers on SiO_2/glass) films

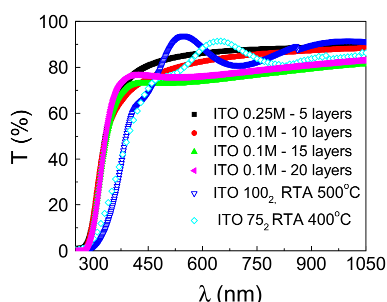

Fig. 7 Transmission of sputtered ITO (75 % N_2, RTA 500 °C and 100 % N_2, RTA 400 °C—solid fill shapes) in comparison with sol–gel ITO (0.1 M– 10, 15 and 20 layers on SiO_2/glass—no fill shapes) films

determined by transmission measurements, are around 3.6–3.9 eV (see Table 2) for both types of films (sputtering and sol–gel).

4 Conclusions

A comparison between the structural, morphological and opto-electrical properties of sputtered ITO films (deposited in 75 and 100 % N_2 atmosphere and annealed at 400, 500 and 600 °C) deposited on fused silica and sol–gel ITO films (0.1 and 0.25 M, with 1–20 layers, annealed at 400 °C) deposited on glass and SiO_2/glass is presented.

A series of deposition parameters have been varied in each case and their degree of influence on the structural and morphological properties as well as their ulterior effect on opto-electrical behavior is discussed in detail. By selecting optimized deposition parameters (75 % N_2, RTA 500 °C for sputtered films and 10 layers from 0.1 M solution of SiO_2/glass for sol–gel films) comparable values for the properties of interest (transmission, resistivity and band gap energy) could be obtained in these two series of films.

The films obtained by sol–gel deposition have a higher porosity (11-19 %) compared to the sputtering method (2–10 %), but comparable transmittance values (85–90 %), proper values of the carrier concentration (10^{20}–10^{21} cm^{-3}) and a similar degenerate semiconductor behavior.

The results of these experiments demonstrated the possibility:

– to select a suitable substrate, sol-concentration and deposition number for predetermined properties needed in a certain application;
– to replace the expensive sputtering method with the low cost sol–gel one in TCO applications, especially when large area samples are required.

Acknowledgments This work was supported by the Romanian PNII-ID-PCE-2011-3-0446 grant. Project EU (ERDF) and Romanian Government that allowed the acquisition of the research infrastructure under POS-CCE (Project INFRANANOCHEM—No. 19/01.03.2009) is also acknowledged.

References

1. V. Malathy, S. Sivaranjani, V.S. Vidhya, T. Balasubramanian, J. Joseph Prince, C. Sanjeeviraja, M. Jayachandran, J. Mater. Sci. Mater. Electron. **21**, 1299 (2010)
2. R.A. Afre, Y. Hayashi, T. Soga, G. Kalita, M. Umeno, Chem. Phys. Lett. **481**, 68 (2009)
3. T. Minami, Thin Sol. Films **516**, 5822 (2008)
4. O. Tuna, Y. Selamet, G. Aygun, L. Ozyuzer, J. Phys. D Appl. Phys. **43**, 055402 (2010)
5. T. Koida, M. Kondo, K. Tsutsumi, A. Sakaguchi, M. Suzuki, H. Fujiwara, J. Appl. Phys. **107**, 033514 (2010)
6. V.V. Pillay, K. Vijayalakshmi, J. Mater. Sci. Mater. Electron. **24**, 1895 (2013)
7. A.S.A.C. Diniz, Renew. Energ. **36**, 1153 (2011)
8. D.S. Ginley, H. Hosono, D.C. Paine, *Handbook of Transparent Conductors* (Springer, New York, 2010)
9. M. Nistor, A. Petitmangin, C. Hebert, W. Seiler, Appl. Surf. Sci. **257**, 5337 (2011)
10. F.O. Adurodija, H. Izumi, T. Ishihara, H. Yoshioka, M. Motoyama, J. Mater. Sci. Mater. Electron. **12**, 57 (2001)
11. M. Gartner, H. Stroescu, A. Marin, P. Osiceanu, M. Anastasescu, M. Stoica, M. Nicolescu, M. Duta, S. Preda, E. Aperathitis, A. Pantazis, V. Kampylafka, M. Modreanu, M. Zaharescu, Appl. Surf. Sci. **313**, 311 (2014)
12. H. Stroescu, M. Anastasescu, S. Preda, M. Nicolescu, M. Stoica, N. Stefan, E. Aperathitis, M. Modreanu, M. Zaharescu, M. Gartner, Thin Solid Films **541**, 121 (2013)
13. G. Zhu, Z. Yang, J. Mater. Sci. Mater. Electron. **24**, 3646 (2013)
14. H. Cho, Y.H. Yun, Ceram. Int. **37**, 615 (2011)
15. M. Hasan, Zadeh Maha, M.M. Bagheri-Mohagheghi, H. Azimi-Juybari. Thin Sol. Films **536**, 57 (2013)
16. S. Marikkannu, C. Sanjeeviraja, S. Piraman, A. Ayeshamariam, J. Mater. Sci. Mater. Electron. **26**, 2531 (2015)
17. C.J. Brinker, G.W. Scherer, *Sol–Gel Science: The Physics and Chemistry of Sol–Gel Processing* (Academic Press Inc., CA, USA, 1990)
18. L. Predoana, S. Preda, M. Nicolescu, M. Anastasescu, J.M. Calderon-Moreno, M. Duta, M. Gartner, M. Zaharescu, J. Sol–Gel. Sci. Technol. **71**, 303 (2014)

19. H.P. Klug, L.E. Alexander, *X-Ray Diffraction Procedure for Polycrystalline and Amorphous Materials*, 2nd edn. (Wiley, New York, 1974)
20. J. Lv, K. Huang, X. Chen, J. Zhu, C. Cao, X. Song, Z. Sun, Opt. Commun. **284**, 2905 (2011)
21. J. Hotovy, J. Hüpkes, W. Böttler, E. Marins, L. Spiess, T. Kups, V. Smirnov, I. Hotovy, J. Kováč, Appl. Surf. Sci. **269**, 81 (2013)
22. V. Senthilkumar, P. Vickraman, M. Jayachandran, C. Sanjeeviraj, Vacuum **84**, 864 (2010)
23. G.B. González, T.O. Mason, J.P. Quintana, O. Warschkow, D.E. Ellis, J.H. Hwang, J.P. Hodges, J.D. Jorgensen, J. Appl. Phys. **96**, 3912 (2004)
24. S. Honda, M. Watamori, K. Oura, Thin Sol. Films **281–282**(1–2), 206 (1996)
25. R. Latz, K. Michael, M. Scherer, Jpn. J. Appl. Phys. **30**(2A), L149–L151 (1991)
26. N. Kikuchi, E. Kusano, E. Kishio, A. Kinbara, H. Nanto, J. Vac. Sci. Technol. A **19**(4), 1636 (2001)
27. P.K. Song, Y. Shigesato, M. Kamei, I. Yasui, Jpn. J. Appl. Phys. **38**(5A), 2921 (1999)
28. E. Kubota, Y. Shigesato, M. Igarashi, T. Haranoh, K. Suzuki, Jpn. J. Appl. Phys. **33**(9A), 4997 (1994)
29. L.J. Meng, M.P. Dos Santos, J. Vac. Sci. Technol. A **18**(4), 1668 (2000)
30. M. Chen, Z.L. Pei, X. Wang, Y.H. Yu, X.H. Liu, C. Sun, L.S. Wen, J. Phys. D Appl. Phys. **33**, 2538 (2000)
31. C.C. Yu, W.H. Lan, K.F. Huang, J. Nanomater. **2014**, 1 (2014)
32. C. Nunes de Carvalho, A. Luis, G. Lavareda, E. Fortunato, A. Amaral, Surf. Coat. Technol. **151–152**, 252 (2002)
33. M. Losurdo, M. Giangregorio, P. Capezzuto, G. Bruno, R. De Rosa, F. Roca, C. Summonte, J. Pla, R. Rizzoli, J. Vac. Sci. Technol. A **20**, 37 (2002)